Supplementary Information

Seamless Integration of Ni Metal–Organic Framework on Three-Dimensional Substrates for Nonenzymatic Glucose Sensing

Haonan Ren[1], Fan Yang[1,*], Meng Cao[1], Bin Shan[2], Rong Chen[1,*]

[1] *State Key Laboratory of Intelligent Manufacturing Equipment and Technology, School of Mechanical Science and Engineering, Huazhong University of Science and Technology, Wuhan 430074, People's Republic of China*

[2] *State Key Laboratory of Materials Processing and Die & Mould Technology, School of Materials Science and Engineering, Huazhong University of Science and Technology, Wuhan 430074, People's Republic of China*

[*] Corresponding authors:

Fan Yang – Email: *fan_yang@hust.edu.cn*

Rong Chen – Email: *rongchen@mail.hust.edu.cn*

Outline

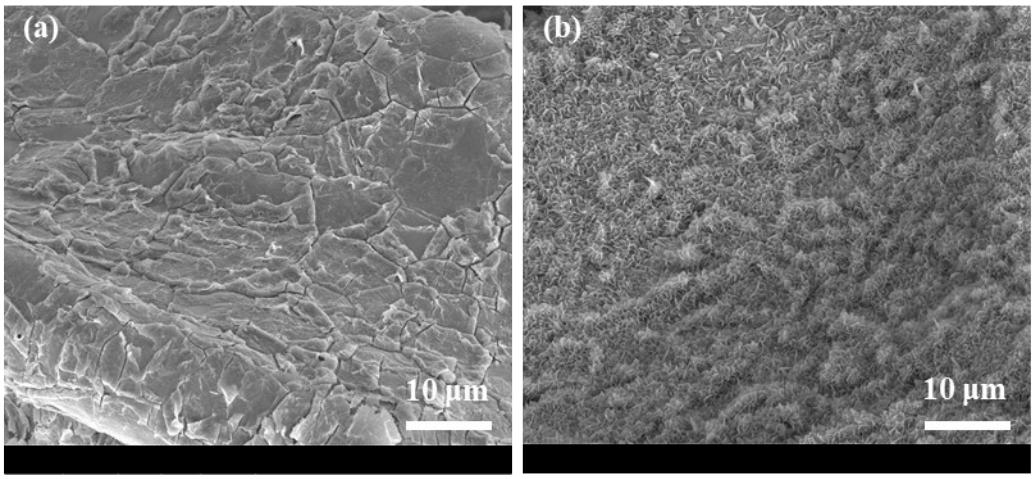

Fig. S1 SEM images (a) NiO/NF and (b) Ni-MOF/NF at a different magnification.

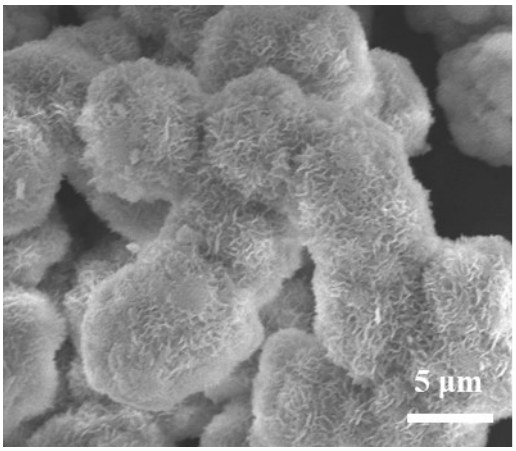

Fig. S2 SEM image of Ni-MOF powder.

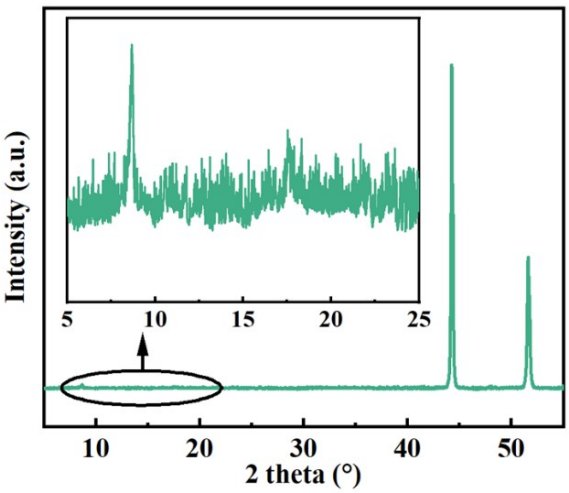

Fig. S3 Full XRD pattern of Ni-MOF/NF.

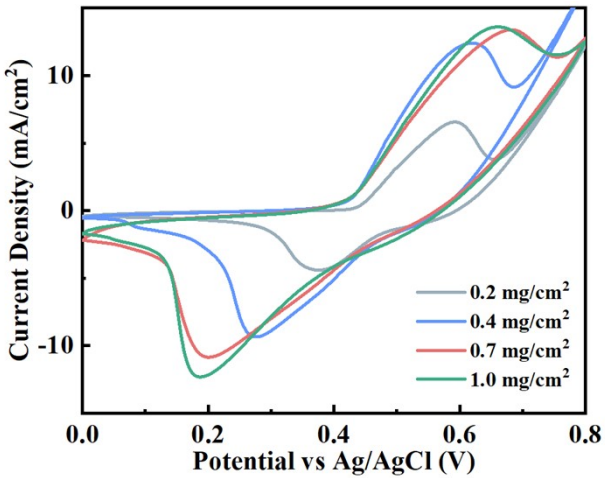

Fig. S4 CV curves of Ni-MOF/NF (DC) electrodes with different loading mass of Ni-MOF powder in 0.1M NaOH with 0.5 mM glucose at scan rate of 30mV/s.

With the increase of loading mass from 0.2 to 0.4 mg/cm^2, the anodic and cathodic peak currents had a significant increase. However, when the loading mass reached 0.7 mg/cm^2 and 1.0 mg/cm^2, CV curves exhibited basically the same characteristics, which are close to that of 0.4 mg/cm^2. Additionally, excessive loading mass could lead to issues including materials delamination and detachment, thereby affecting the reproducibility of the electrode. Consequently, 0.4 mg/cm^2 was selected as the optimal loading mass to drop-cast Ni-MOF/NF (DC) electrode.

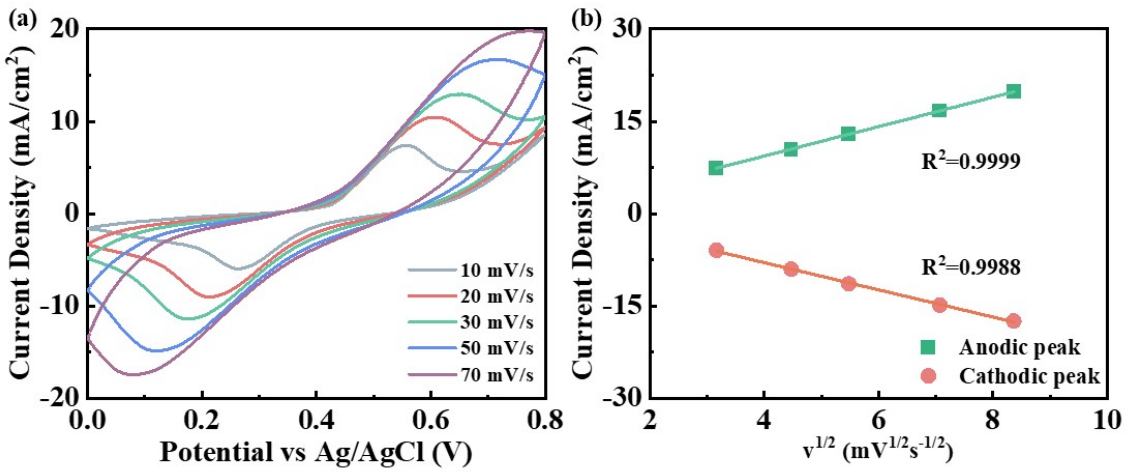

Fig. S5 (a) CV curves of Ni-MOF/NF in 0.1 M NaOH with 0.5 mM glucose at different scan rates. (b) Calibration curves of anodic and cathodic peak current versus the square root of the scan rate.

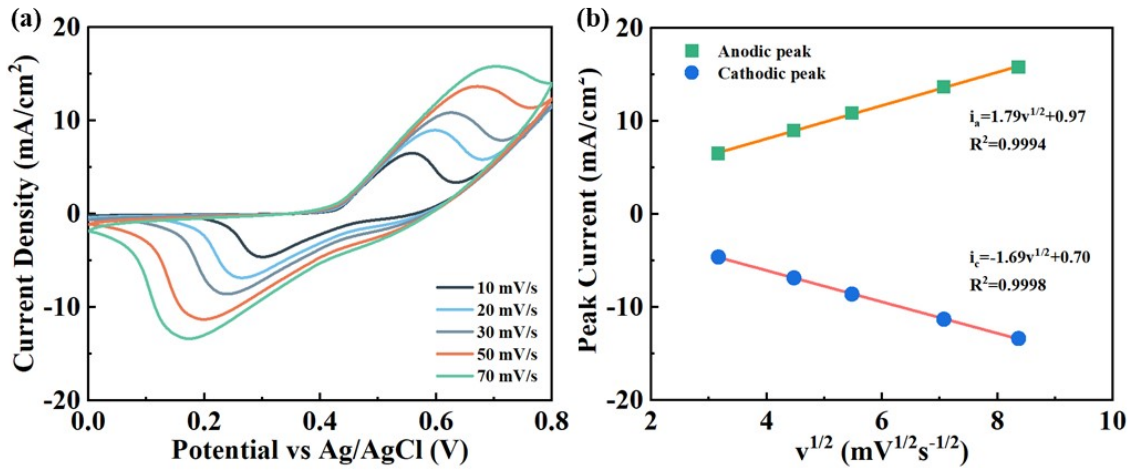

Fig. S6 (a) CV curves of Ni-MOF/NF (DC) in 0.1 M NaOH with 0.5 mM glucose at different scan rates. (b) Calibration curves of anodic and cathodic peak current versus the square root of the scan rate.

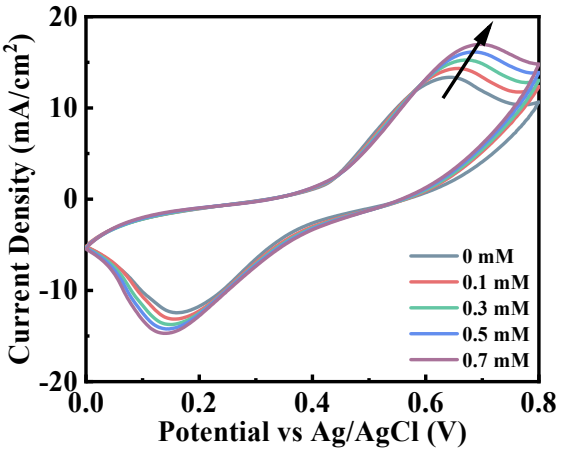

Fig. S7 CV curves of Ni-MOF/NF with different glucose concentrations in NaOH, scan rate: 30 mV/s.

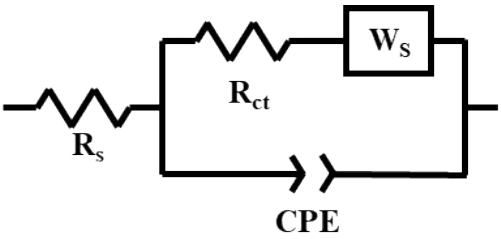

Electrode	R_s (Ω)	R_{ct} (Ω)
Ni-MOF/NF (DC)	12.92	74.28
Ni-MOF/NF	10.84	24.54

Fig. S8 Equivalent circuit diagram and the fitted results of EIS for Ni-MOF/NF and Ni-MOF/NF (DC) in NaOH.

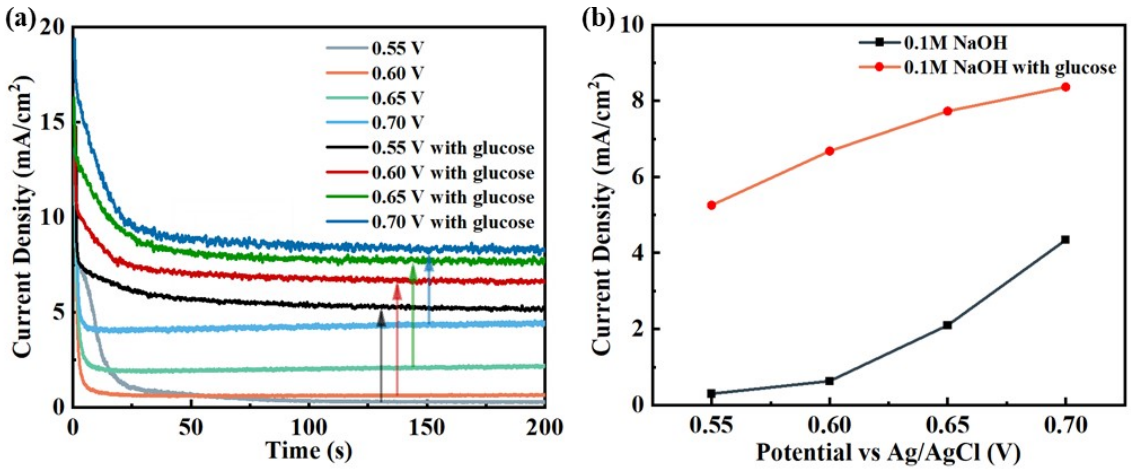

Fig. S9 (a) i-t curves of Ni-MOF/NF with and without 0.5 mM glucose at different potentials. (b) Amperometric responses at different potentials with and without 0.5 mM glucose.

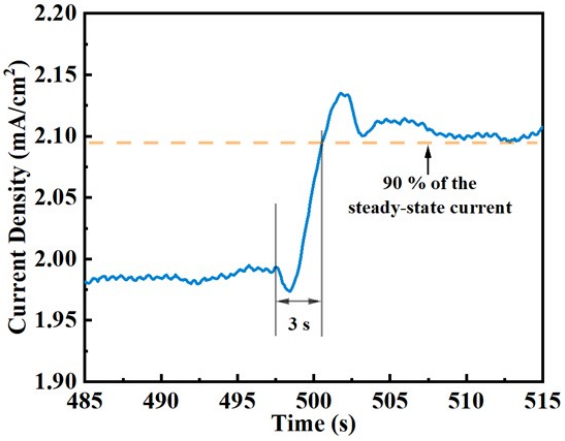

Fig. S10 i-t curve of Ni-MOF/NF at 0.6 V when adding 10 μM of glucose at 500 s.

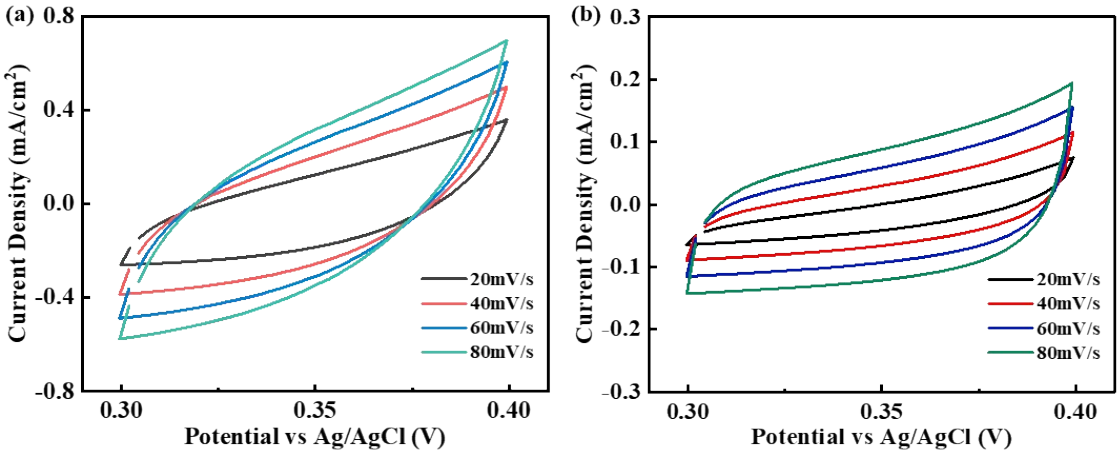

Fig. 11 CV curves of (a) Ni-MOF/NF and (b) Ni-MOF/NF (DC) at different scan rates in the potential range from 0.3 V to 0.4 V in 0.1 M NaOH with 0.1 mM glucose.

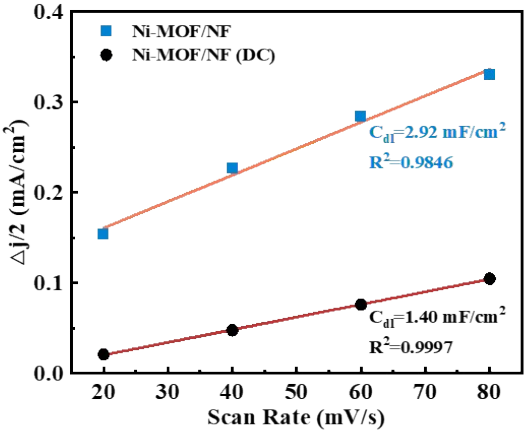

Fig. 12 Calibration curves of the capacitive current density (at 0.35 V) versus scan rate.

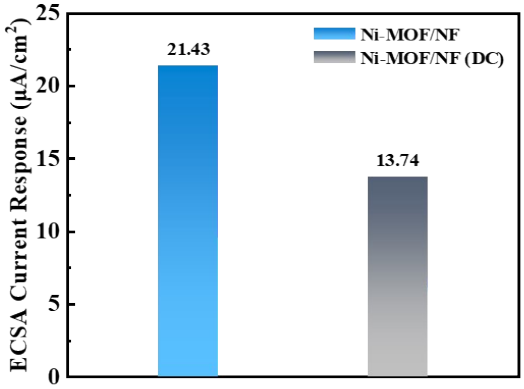

Fig. 13 ECSA normalized current response upon 0.1 mM glucose at 0.6 V.

Table S1 Comparison of nanomaterials-based nonenzymatic glucose sensing electrodes.

Electrode	Sensitivity ($\mu A\ mM^{-1}\ cm^{-2}$)	Linear Range (μM)	LOD (μM)	Electrolyte	Ref.
Ni-MOF/NF	14280	4 ~ 536	2.65	0.1 M NaOH	This work
Co-MOF/NF	10886	1 ~ 3000	0.0013	0.1 M NaOH	[1]
Cu_1Co_2-MOF/NF	8304.4	50 ~ 500	23	0.1 M NaOH	[2]
NF/FLCo-ZIF	2981	2 ~ 1000	0.42	0.1 M NaOH	[3]
NF/ZIF-67@GO/$Co(OH)_2$	2412.7	1 ~ 8546	0.934	1 M KOH	[4]
Ni_3Se_2 NS/NF	5962	0.25 ~ 6335	0.04	0.5 M NaOH	[5]
α-Fe_2O_3/NF	10356	5 ~ 200	0.87	0.1 M NaOH	[6]
Cu(II)-HNFs@NF	2497.1	0.1 ~ 3000	0.03	0.1 M NaOH	[7]
CuO/$Ni(OH)_2$/CC	598.6	50 ~ 8500	0.31	0.1 M NaOH	[8]
Ni/WO_3 MSBs@CC	890	5 ~ 255	0.9	0.1 M NaOH	[9]
CuO polyhedrons/CC	13575	0.5 ~ 800	0.46	0.1 M NaOH	[10]

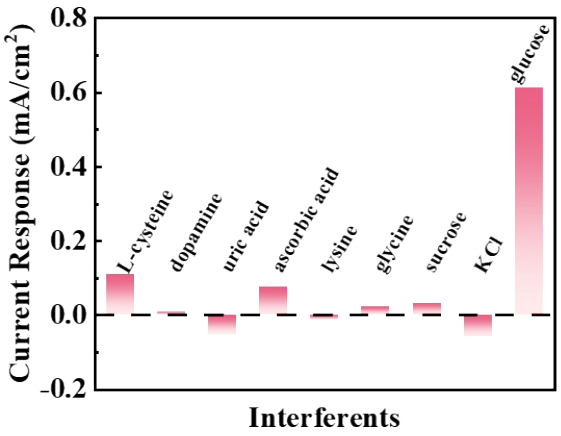

Fig. S14 Current responses of Ni-MOF/NF to different interferents and glucose.

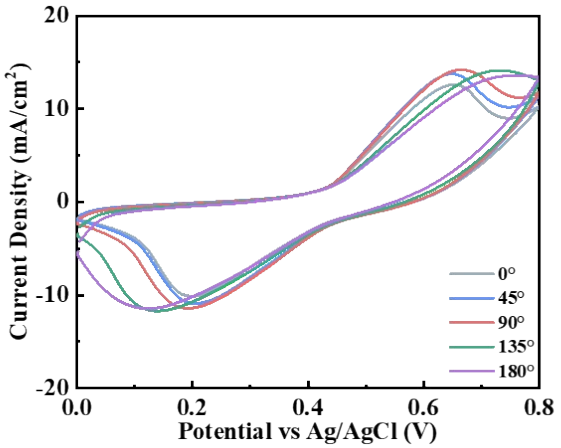

Fig. S15 CV curves of Ni-MOF/NF with 0.5 mM glucose in NaOH at the scan rate of 30 mV·s^{-1} in the condition of different bending angles.

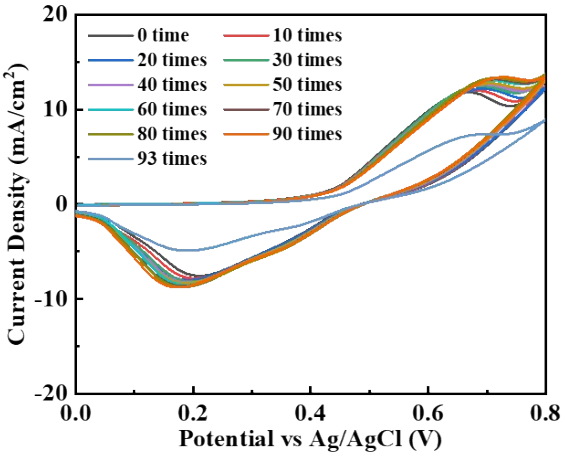

Fig. S16 CV curves of Ni-MOF/NF with 0.5 mM glucose in NaOH at the scan rate of 30 $mV \cdot s^{-1}$ in the condition of different bending counts.

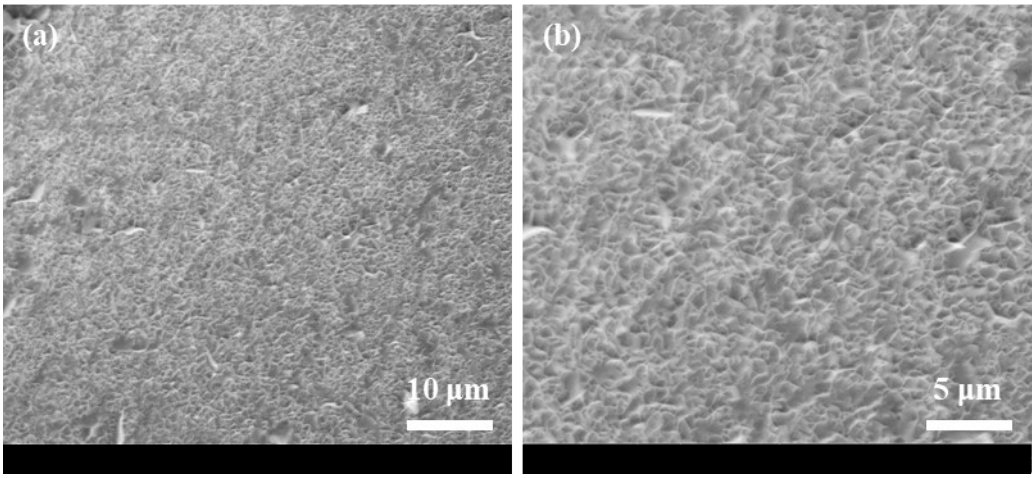

Fig. S17 SEM images of Ni-MOF/NF at (a) low magnification and (b) high magnification.

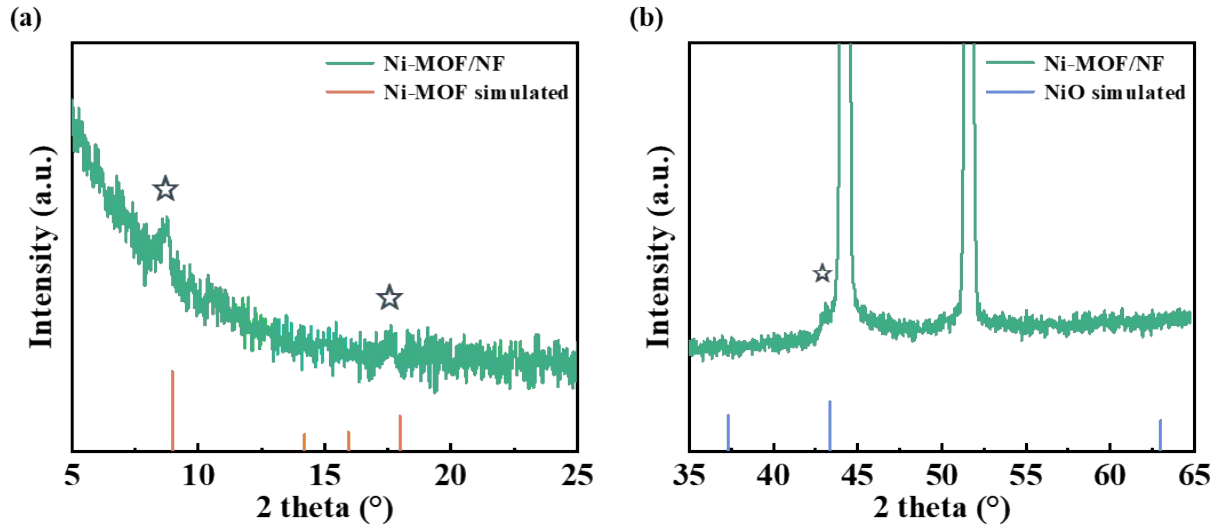

Fig. S18 XRD pattern of Ni-MOF/NF after electrochemical tests at (a) low diffraction angle range and (b) high diffraction angle range.

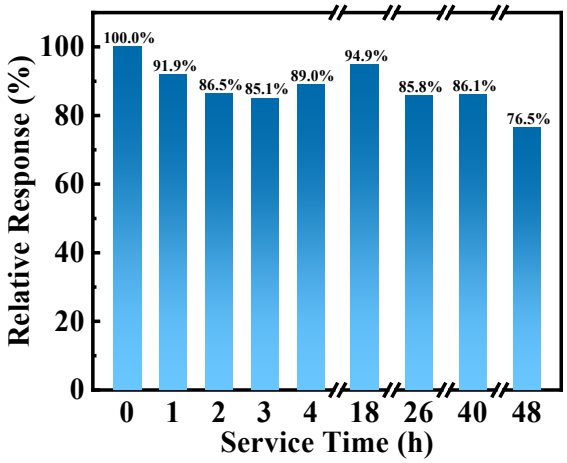

Fig. S19 Service life evaluation by relative response of single electrode to 0.2 mM glucose versus service time.

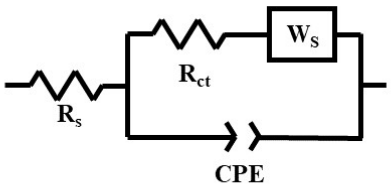

Electrode	R_s (Ω)	R_{ct} (Ω)
Ni-MOF/CP (DC)	22.51	20289
Ni-MOF/CP	21.24	5329

Fig. S20 Equivalent circuit diagram and the fitted results of EIS for Ni-MOF/CP and Ni-MOF/CP (DC) in PBS.

Table S2 Comparison of nonprecious metal nanomaterials-based nonenzymatic glucose sensing electrodes working in neutral condition.

Electrode	Sensitivity ($\mu A\ mM^{-1}\ cm^{-2}$)	Linear Range (μM)	LOD (μM)	Electrolyte	Ref.
Ni-MOF/CP	6.57	200 ~ 7000	198.25	PBS	This work
	4.10	7000 ~ 16000	-		
MAF-5-Co^{II} NSLOD/SPE	24.22	7.81 ~ 250	0.3	PBS	[11]
	1.32	500 ~ 10000	-		
FeBDC-derived Fe_3O_4	4.67	0 ~ 9000	15.7	PBS	[12]
CPNs/GCE	0.00790	1000 ~ 30000	300	PBS	[13]
FTO/[CoFe]	18.69	100 ~ 8200	67	PBS	[14]
Cu NWs-MOFs-GO/GE	7.72	20 ~ 26600	7	PBS	[15]

References

1 Y. Li, M. Xie, X. Zhang, Q. Liu, D. Lin, C. Xu, F. Xie and X. Sun, *Sens. Actuators, B*, 2019, **278**, 126–132.

2 Q. Du, Y. Liao, N. Shi, S. Sun, X. Liao, G. Yin, Z. Huang, X. Pu and J. Wang, *J. Electroanal. Chem.*, 2022, **904**, 115887.

3 P. Arul and S. A. John, *Electrochim. Acta*, 2019, **306**, 254–263.

4 B. Tao, H. Zheng, J. Li, F. Miao and P. Zhang, *Mater. Sci. Eng. B*, 2023, **298**, 116895.

5 M. Ma, W. Zhu, D. Zhao, Y. Ma, N. Hu, Y. Suo and J. Wang, *Sens. Actuators, B*, 2019, **278**, 110–116.

6 Y. Liu, W. Zhao, X. Li, J. Liu, Y. Han, J. Wu, X. Zhang and Y. Xu, *Appl. Surf. Sci.*, 2020, **512**, 145710.

7 P. Ma, R. Bi, Q. Wang, L. Lu, X. Ma and F. Chen, *Mater. Res. Bull.*, 2024, **170**, 112583.

8 S. Sun, N. Shi, X. Liao, B. Zhang, G. Yin, Z. Huang, X. Chen and X. Pu, *Appl. Surf. Sci.*, 2020, **529**, 147067.

9 C. Wang, L. Du, X. Xing, D. Feng, Y. Tian, Z. Li and D. Yang, *Appl. Surf. Sci.*, 2022, **586**, 152822.

10 S. Cheng, X. Gao, S. DelaCruz, C. Chen, Z. Tang, T. Shi, C. Carraro and R. Maboudian, *J. Mater. Chem. B*, 2019, **7**, 4990–4996.

11 M. Adeel, V. Canzonieri, S. Daniele, A. Vomiero, F. Rizzolio and Md. M. Rahman, *Microchim. Acta*, 2021, **188**, 77.

12 S. A. Abrori, N. L. W. Septiani, Nugraha, I. Anshori, Suyatman, V. Suendo and B. Yuliarto, *Sensors*, 2020, **20**, 4891.

13 P. P. Tomanin, P. V. Cherepanov, Q. A. Besford, A. J. Christofferson, A. Amodio, C. F. McConville, I. Yarovsky, F. Caruso and F. Cavalieri, *ACS Appl. Mater. Interfaces*, 2018, **10**, 42786–42795.

14 R. Chalil Oglou, T. G. Ulusoy Ghobadi, E. Ozbay and F. Karadas, *Anal. Chim. Acta*, 2021, **1188**, 339188.

15 G. Zang, W. Hao, X. Li, S. Huang, J. Gan, Z. Luo and Y. Zhang, *Electrochim. Acta*, 2018, **277**, 176–184.